Dalton Transactions

ROYAL SOCIETY OF CHEMISTRY

PAPER

View Article Online
View Journal | View Issue

Cite this: *Dalton Trans.*, 2023, **52**, 7684

A proficient multivariate approach for iron(II) spin crossover behaviour modelling in the solid state†

Lorenzo Marchi, [a] Simone Fantuzzi, [a] Andrea Cingolani,[b] Alessandro Messori,[b] Rita Mazzoni, [b] Stefano Zacchini, [b] Marina Cocchi [a] and Luca Rigamonti *[a]

Received 20th March 2023,
Accepted 2nd May 2023

DOI: 10.1039/d3dt00847a

rsc.li/dalton

Iron(II) *bis*-pyrazolilpyridyl (bpp-R) complexes $[Fe(bpp\text{-}R)_2](X)_2$·solvent, R = substituent and X^- = anion, can undergo a spin transition from high (S = 2, HS) to low spin (S = 0, LS), being spin crossover (SCO) in the solid state. The distortion of the octahedral coordination environment around the metal centre is governed by crystal packing, *i.e.* the intermolecular interactions among the substituent R of the bpp-R ligands, the anion X^-, and the co-crystallized solvent, and this modulates the SCO behaviour. In this work, an innovative multivariate approach, through the combination of the chemometric tools Principal Component Analysis and Partial Least Squares regression, was applied on the coordination bond distances and angles and selected torsional angles of the available HS structures. The obtained results can efficiently model and rationalize the structural data distinguishing between SCO-active and HS-blocked complexes bearing different R groups, X^- anions, and co-crystallized solvents and help predict the spin transition temperature $T_{1/2}$.

Introduction

Molecular magnetic bistability in spin crossover (SCO) transition metal complexes has been intensively studied for the last few decades,[1–5] and it mostly involves the thermally induced rearrangement of d electrons from a high spin (HS) to a low spin (LS) state in metal ions with d^4–d^7 configuration and an octahedral coordination environment.[6–8] SCO materials have gained popularity because of their flexibility in controlling the spin transition under different types of external stimuli like temperature, pressure, or light and X-ray irradiation,[5,7,9–12] and application of bistable systems like SCO complexes can be made in the field of electronics and engineering as sensors, memory supports, and quantum computers.[3,4,13] The existence of HS and LS species is also fundamental in living systems, where the active sites of metal enzymes and proteins can show the change of the spin state upon regulation of their biological activity.[14–16]

The scenario of SCO compounds is dominated by octahedral iron(II) derivatives mostly with nitrogen-donor ligands[7,13,17,18] where the d^6 configuration allows a spin transition from HS with S = 2 to LS with S = 0, also accompanied by changes in the colour,[19] dielectric constant,[20] and electrical resistance.[21] The spin switch in iron(II) also shows the greatest structural differences from the HS state with long Fe–N bonds (2.15–2.20 Å) to the LS state with short Fe–N bonds (1.90–1.95 Å), and this makes iron(II) compounds the most desirable platform for studying the cooperativity in spin transitions and structure–function relationships,[8] guided by the electronic features of the substituents on the coordinated

[a]*Dipartimento di Scienze Chimiche e Geologiche, Università degli Studi di Modena e Reggio Emilia, via G. Campi 103, 41125 Modena, Italy.*
E-mail: luca.rigamonti@unimore.it
[b]*Dipartimento di Chimica Industriale 'Toso Montanari', Università degli Studi di Bologna, viale Risorgimento 4, 40136 Bologna, Italy*

†Electronic supplementary information (ESI) available: Rules for the three-letter labels of the iron(II) complexes (Table S1); drawing of the substituent R of complexes $[Fe(bpp\text{-}R)_2](X)_2$·solvent with relative letter + number coding and anions $[Ni(mnt)_2]^-$ and $[Co(carborane)_2]^-$ (Fig. S1); $[Fe(bpp\text{-}R)_2](X)_2$·solvent complexes known in the literature (Table S2); the 28 structural parameters considered for building the PCA and PLS models (Table S3); Chemometric methods; Experimental section; crystallographic and refinement data for **C01AA** at 100 and 293 K (Table S4); coordination bond distances and angles of **C01AA** at 100 and 293 K (Table S5); PC1 *vs.* PC2 scores plots for the PCA model constructed including all the variables D, A and T for the selected 84 HS complexes, with symbols corresponding to the R groups, anions X^-, and co-crystallized solvents (Fig. S2–S4); PC1 *vs.* PC2 loadings plot for the PCA model constructed including all the variables D, A, and T for the selected 83 HS complexes (Fig. S5); PC1 *vs.* PC2 loadings plot for the PCA model constructed including all the variables D, A, and T for the selected 39 solvent-free (SF) HS complexes (Fig. S6); PC1 *vs.* PC2 scores and loadings plots for the PCA model constructed including all the variables D, A, and T for the 17 HS complexes with R = *Si*Pr (Fig. S7); root mean square errors in calibration (RMSEC) and in cross-validation (RMSECV) *vs.* latent variable number plot (Fig. S8); a PLS regression model based on 34 structures of iron(II) complexes: weights plot LV1 *vs.* LV2 (Fig. S9); $T_{\frac{1}{2}}$ value distribution in the PC1 *vs.* PC2 scores plots across the PCA models constructed with either the 83 HS complexes or the 39 SF HS derivatives (Fig. S10). CCDC 2191546 and 2191547. For ESI and crystallographic data in CIF or other electronic format see DOI: https://doi.org/10.1039/d3dt00847a

ligands and the intermolecular interactions,[22,23] also with the employment of machine learning.[24,25]

The iron(II) complexes $[Fe(bpp\text{-}R)_2](X)_2$·solvent bearing two *mer*-coordinated neutral tridentate nitrogen-donor bpp-R ligands (2,6-*bis*(pyrazol-1-yl)pyridine substituted at position 4 of the pyridyl ring with various R groups), different X^- anions, and co-crystallized solvent, if present, have attracted much attention for their peculiar SCO properties through the past two decades.[5,26–83] The perfect octahedral coordination is not achievable due to the intrinsic structure of the ligands, which makes the *trans*-N(pyrazole)-Fe–N(pyrazole) bite angle, ψ, within the same bpp-R always around 145–150°, much lower than 180°. Furthermore, these complexes are structurally characterized by the *trans*-N(pyridine)–Fe–N(pyridine) angle, ϕ, and the dihedral angle between the least squares (l.s.) planes described by the 16 C/N atoms of the bpp-R ligands, θ (Scheme 1), which can be far from the values of a regular octahedron (ϕ = 180° and θ = 90°).[41,56] The intermolecular interactions among the $[Fe(bpp\text{-}R)_2]^{2+}$ cations, the anions X^-, and the co-crystallized solvent govern the iron(II) distortion degree and hence the SCO behaviour of a given complex in the solid state in the light of the required ligand rearrangement from the expanded HS to the compressed LS states, *i.e.* the ability of a lattice to accommodate such changes.[8] A recent work has proposed a structure–function relationship relating the magnetic bistability features of the iron(II) centres with the structural variability upon switching from HS to LS through the three indices V_{oh}, Σ and Θ, where V_{oh} = volume of the FeN_6 octahedron, $\Sigma = \sum_{i=1}^{12} |90 - \beta_i|$ (β_i are the 12 *cis*-N–Fe–N angles about the iron atom) and $\Theta = \sum_{j=1}^{24} |60 - \gamma_j|$ (γ_j are the 24 unique N–Fe–N angles measured on the projection of two triangular faces of the octahedron along their common pseudo-3-fold axis), and their variation upon spin transition.[84]

The three indices V_{oh}, Σ and Θ are basically derived from coordination bond distances and angles, what we can call the original variables, which are in turn governed by the crystal packing. The number of known iron(II) crystal structures with bpp-R ligands is above 250, either in the LS or in the HS state, meaning thousands of original variables. Table S1 in the ESI† reports a three-letter label rule able to encode the complexes, Fig. S1 in the ESI† contains the graphical representation of the different substituents R, and Table S2 in the ESI† lists the derivatives with relevant information. The effective rationalization and modelling of the information these compounds provide could be of great interest. To this aim, the structural data, despite their large amount, can be efficiently handled by chemometrics. Thus, here we are proposing a unified multivariate analysis of the coordination structural parameters of derivatives $[Fe(bpp\text{-}R)_2](X)_2$·solvent considering all the complexes as a unique dataset (ensemble), aiming at studying and modelling the coordination distortion in relation to the SCO properties in the first place, and then trying to predict properties like the spin transition temperature, $T_{1/2}$. A comparable approach has been recently proposed on DFT-calculated steric and electronic descriptors of a series of ligands employed in metal complexation for the analysis and prediction of catalytic behaviour.[85,86]

The six torsional angles (T1–T6) involving the pyridyl and pyrazolyl rings and the dihedral angle θ (T_LL) were considered in addition to the six coordination bond distances (D1–D6) and the fifteen coordination bond angles (A1–A15) as probes of the effects of the crystal packing in the solid state on the distortion of the coordination environment (see Table S3 in the ESI† for the definition of D, A, and T, and Results and discussion for further details). The multivariate approach through Principal Component Analysis (PCA)[87] and Partial Least Squares (PLS)[88] regression (see Chemometric methods in the ESI†) will lead to complete and general comprehensive models of the overall influence of R, X^-, and the co-crystallized solvent on the observed structural features of the different iron(II) complexes and then on their magnetic behaviour. PCA was used as an exploratory analysis method to rationalize the available literature data and study the interplay of the structural factors, and PLS was applied in the second part of the study for attempting the prediction of magnetic properties.

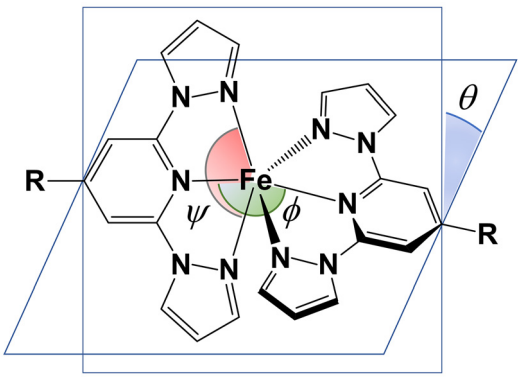

Scheme 1 Molecular scheme of $[Fe(bpp\text{-}R)_2]^{2+}$ complexes, highlighting the θ, ϕ and ψ angles.

Results and discussion

Structural data for complexes with bpp-Me

The magnetic properties of the iron(II) complexes with bpp-Me, which is among the ligands with the smallest R group except the unsubstituted bpp-H, appeared to be noteworthy, since these compounds show a strong dependency of the SCO behaviour from the anion X^-.[59] The solvent free (SF) structure of **C01AA** could not be achieved from the $MeNO_2$: Et_2O solvent combination during the crystallization process, and the solvated **C01AC** was predominant. The synthesis was here repeated changing the crystallization mixture to MeCN : Et_2O, analogous to the COOMe case,[68,89] and only **C01AA** could luckily be isolated as yellow crystals suitable for X-ray diffraction. Details on the synthesis and structure collection and refinement at 100 and 293 K are reported in the Experimental section and in Table S4 in the ESI,† while Fig. 1 contains the

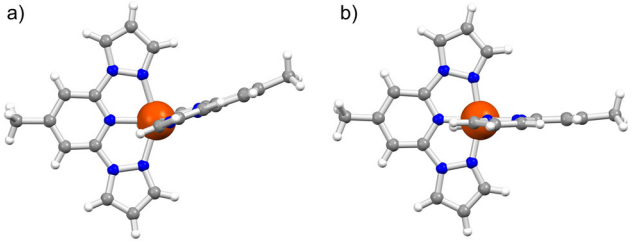

Fig. 1 Perspective view of the structure of the $[Fe(bpp\text{-}Me)_2]^{2+}$ cation in **C01AA** in the (a) HS (293 K) and (b) LS (100 K) states. The anions BF_4^- are omitted for clarity; colour code: Fe = orange, N = blue, C = grey, H = white.

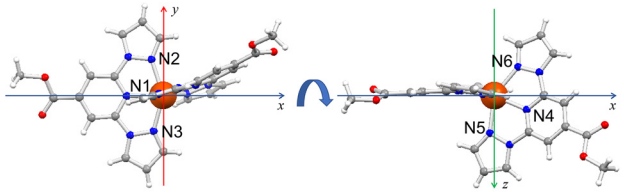

Fig. 2 Definition of the cartesian reference frame for $[Fe(bpp\text{-}R)_2]^{2+}$ cations, using R = COOMe as representative,[68] and labelling of the 6 nitrogen atoms coordinated to the iron(II) centre; colour code: Fe = orange, O = red, N = blue, C = grey, H = white.

perspective depiction of the cation $[Fe(bpp\text{-}Me)_2]^{2+}$ in its HS and LS states. Coordination bond distances and angles are collected in Table S5 in the ESI,† and it is possible to observe how the distortion angles ϕ and θ (164.85(15)° and 89.64°, respectively, at 293 K) are very close to the ones of **C01BA** (163.7(2)° and 89.48(7)° at 240 K), confirming the similarity of the SCO behaviour with that of **C01AA**.[59] The structural data of this complex, which shows a pronounced Jahn–Teller distortion that usually inhibits SCO, are fundamental for building our models, since they represent an "unexpected case" when looking at the single parameters.

Dataset assembly and PCA models

The construction of a sound and robust dataset is the essential part for chemometric multivariate models. Treating HS and LS compounds together would help discriminate the HS complexes from the LS ones, but this is clear from the Fe–N bond distances. The ligand field in this family should be comparable, since the overall donor ability of the two bpp-R ligands is tuned only by the presence of R, but its electron donating or withdrawing power would not be able to modulate the ligand field up to make it too weak to promote SCO, as Halcrow showed with his solution studies.[63] In the light of this point, only HS structures were then considered aiming to distinguish among the complexes able to undergo spin transition and the ones blocked in the HS state due to crystal packing effects. The parameters of the 83 HS species among the 250 HS/LS crystal structures determined and available from the Cambridge Crystallographic Data Centre (CCDC)[90–93] (see Table S2 in the ESI† for all details) were then retrieved and collected.

After that selection, an *ad hoc* nitrogen atom numbering rule was applied to achieve a unique correspondence between structures belonging to different space groups and symmetries. This also gave the opportunity to compare compounds regardless of the original naming and orientation. This step is fundamental to avoid the introduction of fake sources of variance in the model. The classification rules of the six nitrogen atoms are reported below and depicted in Fig. 2 using $[Fe(bpp\text{-}COOMe)_2]^{2+}$ as the template:[68]

1. the bpp-R ligand with the shortest Fe–N(py) distance is positioned on the left side and in the plane of the screen; the pyridyl nitrogen atom of this bpp-R ligand becomes N1, while the pyridyl nitrogen atom of the second bpp-R ligand is N4;

2. The molecule is positioned so that the second bpp-R ligand is inclined upward, and this defines N2 and N3 in the first bpp-R ligand;

3. The molecule is now rotated of 90° around the *x* axis, the nitrogen atom of the pyrazolyl ring closer to the *z* axis (or to the first bpp-R ligand) is N5 while the other nitrogen atom is N6.

The 28 structural parameters (original variables) considered for the 83 selected HS complexes, as anticipated in the Introduction, and reported in Table S3 in the ESI,† are the following:

- The six Fe–N coordination bond distances (named from D1 to D6 and following the numbering rule of the coordinated nitrogen atoms);
- The fifteen N–Fe–N coordination angles (named from A1 to A15, A3 being the angle ϕ);
- Six torsional angles comprising the aromatic rings of the ligands in the complex (T1–T6);
- The torsional angle θ between the l.s. planes of the two ligands (T_LL).

The inclusion of the tortional angles T1–T6 helps considering the deviation from strict planarity caused by rotation around the two C–N pyridine-pyrazole connecting bonds of the bpp-R ligands. This can be in turn related to the crystal packing, which can force some tortional degree within the structure of the $[Fe(bpp\text{-}R)_2]^{2+}$ cations.

PCA extracted information from the 28 variables that describe the 83 HS complexes by rotating the original space in a constructed space so that each new variable, called a principal component (PC), is orthogonal to the others, and that each new variable explains the maximum possible fraction of variance of the data not yet explained by the previous PCs. The PCs are linear combinations of the original variables, the first PC is in the direction of maximum variability of the data, the second is uncorrelated with the first (the two axes are orthogonal) and explains the maximum residual variance fraction, and so on (see the ESI† for further details regarding the PCA and loadings/scores plots interpretation). Block-scaling to unit block variance was applied as preprocessing in our dataset (considering as distinct blocks the D, A and T types of parameters) for the construction of the PCA model, and four PCs contributed to about 74% of the total variance.

PCA, being an unsupervised data analysis tool, allows inspection of the main sources of variability and the "natural" grouping tendencies in the data without imposing any *a priori* information. From the PC1 *vs.* PC2 scores plots (Fig. S2–S4 in the ESI†) we cannot recognize any specific grouping based on R, X^- or solvent. This should not be surprising since the variability sources introduced in the model by 32 substituents, 10 counterions (BF_4^- for 43 complexes and ClO_4^- for 25 complexes, 80% of all the complexes) and 11 co-crystallized solvents (Tables S1 and S2 in the ESI†), true expression of the intermolecular interactions and crystal packing effects we sought for, together contribute to the observed location of the samples in these plots. This brings up the absence of big and well-defined clusters, even if it is possible to observe small grouping of complexes in each single class of R, X^- and solvent, like for example the complexes with substituent S*i*Pr (depicted by brown diamonds in Fig. S2 in the ESI†) concentrated in the centre of the PCA plot.

On the other hand, the model shows a differentiation according to the SCO property of the complexes mostly along PC1 (Fig. 3), with a good distinction between the SCO-active (Y = green squares) and the HS-blocked (N = red diamonds) derivatives. There are cases for which the SCO properties were not studied (N.A. = blue triangles),[50,56,62,63] but based on our model we can confidently envisage that both **O01AF**[62] and **C35AC**[56] (the two complexes in blue triangles in the midst of red diamonds in Fig. 3) are most probably HS-blocked. Spin conversion was detected to be incomplete (partial = light blue triangle) in other complexes,[66,70,82] mainly related to conformational rearrangements of the R groups upon temperature change (S*i*Pr: **S03BC** and **S03BE**,[66] S*t*Bu: **S04AC**[82] and NHCOMe: **N04AE**[70]), hence modification of the intermolecular interactions especially with solvents like $MeNO_2$ and Me_2CO, or reversible solvation processes (*E*-CH=CH–Fc: **C45AG**[36]).

SF **S03AA**[64] and **S03BA**[66] with S*i*Pr as the substituent are instead reported to be able to give spin conversion but are located in the PCA area of the model dominated by the complexes blocked in the HS state. The flexibility of the substituent can be again envisaged as one of the possible causes to justify their place in the plot; in fact, in both complexes one of the two S*i*Pr groups was found to be strongly disordered in the HS structures, while no disorder can be found in the LS ones. An anomaly is also given by the HS-blocked **N04BE**, placed in the SCO-active area of the model, but breaking of the crystallographic symmetry is reported to occur at a temperature close to the expected $T_{1/2}$, similar to that in **N04AE**, and this causes the alteration of the SCO classification.[70]

It is important to point out how there are complexes whose structural data are available at different temperatures, for example the structure of **H01AA** was collected and refined at 375,[26] 300[34,42] and 290[26] K, and all of them were included in the construction of the PCA model. Looking at their position in the PC1 *vs.* PC2 scores plot (Fig. S2 in the ESI†), the four structures of **H01AA** can be found close to each other but with a diagonal shift, tracing both the effect of the temperature at which the crystal structures were collected (T_{RX}) and the goodness of fit of the structural data. This validates our model, which can efficiently consider this degree of variability intrinsically introduced during X-ray diffraction data collection and thus independent and not artificially induced by the model itself.

Noteworthy can be a further comment on the complexes without any substituent (R = H, **H01**) where the $[Fe(bpp\text{-}H)_2]^{2+}$ cation has the smallest dimension and the possible intermolecular interactions do not involve any substituent, which can be instead quite big in some instances (Fig. S1 in the ESI†). This is the case where the most diverse X^- anions are represented, being BF_4^- (**A**),[26,34] ClO_4^- (**B**),[30] PF_6^- (**D**),[27] SbF_6^- (**F**),[30] I^-/I_3^- (**H**),[31] $[Ni(mnt)_2]^-$ (**I**),[45] and [Co(carborane)]$^-$ (**J**).[31] The different dimensions and intermolecular interactions, which each anion can give rise to, lead to a position in two distinct areas of the PC1 *vs.* PC2 scores plot (Fig. S2 and S3 in the ESI†). Complexes with ClO_4^-, PF_6^- and SbF_6^- represent the most extreme examples along the positive PC1 direction, while the other ones seem to be positioned along a diagonal from the negative PC1/PC2 quadrant to the positive PC1/PC2 quadrant, with **H01IC** ($[Ni(mnt)_2]^-$) on the first extreme, **H01AA** (BF_4^-) in the middle and **H01JC** ([Co(carborane)]$^-$) and **H01HA** (I^-/I_3^-) on the other extreme. Even if the molar volumes of BF_4^- and ClO_4^- are quite similar,[94] **H01AA** and **H01BA** are distinct in the model as a clear detection of the different intermolecular contacts, which indeed block **H01BA** in the HS state while allowing **H01AA** to undergo spin conversion at $T_{1/2}$ = 260 K.[26]

The PC1 *vs.* PC2 loadings plot (Fig. S5 in the ESI†) shows how the structural parameters influence the position of the complexes in the scores plot. The greatest contribution to the distinct SCO behaviour is given by the variables that show high loadings values (both positive and negative) on PC1: for example, high values of T_LL (θ) and A3 (ϕ) are directly correlated to SCO = Y, a fact that reflects the most influential structural parameters also reported in the literature within univariate data analyses.[41,56] Nevertheless, these are not the only structural parameters determining the distinction along PC1:

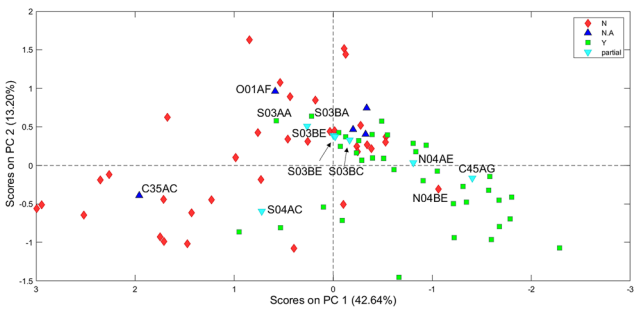

Fig. 3 PC1 *vs.* PC2 scores plot for the PCA model constructed including all the variables D, A and T for the 83 HS complexes; a symbol legend corresponding to the possibility of undergoing spin transition (Y = yes in green, N = no in red, partial in light blue and N.A. in blue) was applied, and the labels are added only for complexes directly discussed in the text.

high values of D1, D2, D4 and D5 also have a direct specific weight in determining the HS-blocked complexes, together with A5 and A10, *i.e.* the two largest *cis-N*(pyridine)–Fe–N(pyrazole) angles between the two coordinated ligands. In contrast, A4 and A7, *i.e.* the two smallest *cis*-N(pyridine)–Fe–N(pyrazole) angles, have the opposite effect compared to A5 and A10, in line with the *mer* coordination of the ligands: low values of A4 and A7 are correlated to lack of SCO transition. It is also interesting to note how D3 and D6 do not have a relevant effect, being close to 0 along PC1, and this is a direct consequence of the rigidity of the bpp-R ligands, but also an indirect confirmation of the good choice of the reference frame in determining the labelling of the nitrogen atoms.

Co-crystallized solvent can be challenging in the engineering of SCO materials.[95] The most interesting aspect in this regard is indeed the improved modelling when the structural parameters of the 39 SF derivatives are considered, representing about half of the previous dataset. The new PCA model implies the same preprocessing as before and considers four PCs, which express 85% of the total variance. In the PC1 *vs.* PC2 scores plot (Fig. 4), the complexes able to undergo spin transition (Y, green square) are well separated from the complexes blocked in their HS state (N, red diamonds). Only **S03AA** and **S03BA**, *i.e.* two complexes bearing S*i*Pr as the substituent and BF_4^- or ClO_4^- as anion,[64,66] are borderline within the model, but as previously outlined this is probably caused by the different conformations of S*i*Pr, which are reported to affect the spin state.[81,96] The PC1 *vs.* PC2 loadings plot (Fig. S6 in the ESI†) is practically superimposable with the one of the all-in PCA model (Fig. S5 in the ESI†), meaning that the considered structural parameters solidly operate in the same way in the two PCA models, and hence the crystal packing effects are efficiently represented by considering the coordination environment of the iron(II) ions.

The usefulness of the chemometric approach can be underlined in the explanation of the case cited before: **C01AA** resides close to **C01BA**, and it is well described by the model, so it can be now moved from an "unexpected" case to a well "modelized" one. With this regard, the presence of the substituent Me, which is the smallest substituent R after its total absence, is already sufficient to modulate the intermolecular contacts in the crystal packing, and **C01AA** and **C01BA**, both SCO-active with similar $T_{1/2}$ values despite the different anion,[59] do not behave as **H01AA** and **H01BA** (R = H), where going from BF_4^- to ClO_4^- blocks the iron(II) in the HS state.[26,30]

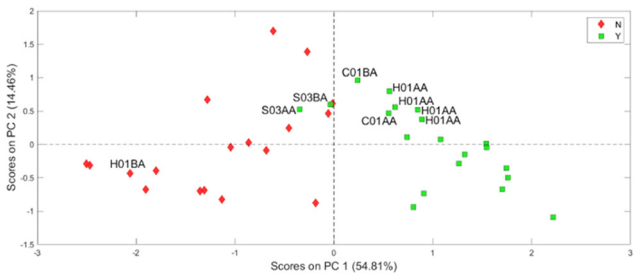

Fig. 4 PC1 *vs.* PC2 scores plot for the PCA model constructed including all the variables D, A and T for the 39 SF HS complexes; a symbol legend corresponding to the possibility of undergoing spin transition (Y = yes in green, N = no in red) was applied, and the labels are added only for complexes directly discussed in the text.

The S*i*Pr substituent, due to the high number of structurally characterised solvated complexes,[64,66,81] represents a good opportunity to create another model with the same R and variable anion X^-, BF_4^- or ClO_4^-, and co-crystallised solvent, Me_2CO, $MeNO_2$, MeCN, EtCN, H_2O or SF. The PCA was conducted on a dataset composed of all 28 structural parameters for 17 **S03** complexes (same preprocessing, four PCs describing the 87% total variance) and the results are reported in Fig. S7 in the ESI.† The PC1 *vs.* PC2 scores plot shows how this model can efficiently cluster the complexes depending on the co-crystallized solvent. Furthermore, PC1 seems to distinguish the steric effect of the co-crystallized solvent, going from EtCN to SF, passing through H_2O, MeCN, $MeNO_2$ and Me_2CO. On the other hand, PC2 seems to represent the different polarities of the solvents, going from the most polar water to the less polar acetone, and maintaining the SF complexes close to 0 of the PC2 axis. Both effects contribute with a comparable and substantial weight to the model, with PC1 and PC2 describing the 36.74% and 25.07% variance, respectively. The two anions BF_4^- and ClO_4^-, instead, have a minor contribution. Nevertheless, a closer look reveals how the perchlorate derivatives are distinguishable from the tetrafluoroborate ones in a diagonal fashion from negative PC1 to positive PC2 for H_2O, MeCN, $MeNO_2$ and Me_2CO solvates, while it is the opposite for the SF derivatives. This highlights how the model can depict and model the presence of intermolecular solvent–anion interactions, absent in the SF structures and different between BF_4^- and ClO_4^-, able to govern the structural distortion of the iron(II) centres.

The most important part of this PCA model is the PC1 *vs.* PC2 loadings plot (Fig. S7 in the ESI†). Indeed, T_LL (θ) and A3 (ϕ), pillars for the previous models, have a much minor role with respect to the torsion angles T2, T3 and T5 this time. This should not be surprising since we are now always considering the same cation with S*i*Pr. On the other hand, this clearly reflects the interlocking of solvent molecules and anions mainly in the pockets between the two *mer* ligands, leading to a mutual rotation of the bpp-R three-ring skeleton along with the C–N bonds. These subtle distortions, induced by the crystal packing, are again proficiently modelled by considering the structural parameters around the iron(II) ions.

PLS regression for $T_{1/2}$ prediction

Another foundation of this work is the construction of predictive models of the SCO properties of iron(II) complexes using their structural properties (D, A and T). A PLS regression model between structural data available in the literature (X-block: 34 × 28) and the temperature $T_{1/2}$ at which they undergo SCO (Y-block: 34 × 1) was then elaborated (see the ESI† for further details regarding the PLS). $T_{1/2}$ was reported

only for 34 complexes over the 83 ones employed for the PCA models (meaning that all the other structures either are double data at different T_{RX}, belong to derivatives blocked in the HS state or that undergo partial SCO, or were not magnetically characterized), so the analysis had to be inevitably restricted to those. Autoscaling was used as preprocessing, and 2 PLS latent variables (LVs) were chosen (Fig. S8 in the ESI†), according to root mean squares error in internal cross validation, *i.e.* RMSECV (using as cancelation scheme a venetian blind with 10 splits). The following results were obtained: RMSEC: 29.3, RMSECV: 37.6, R^2 Cal: 0.76 and R^2 CV: 0.62, where RMSEC and RMSECV are the errors in fit and in cross-validation, respectively, R^2 Cal and R^2 CV are the corresponding coefficients of determination. The predicted (in cross validation) *vs.* experimental $T_{1/2}$ plot is shown in Fig. 5.

RMSECV, albeit being of the same magnitude, is about 5% higher than RMSEC, meaning that the model is not sufficiently rugged. Even though the coefficient of determination in calibration (R^2 Cal) is high, signifying that the calibration has a satisfying goodness of fit, the coefficient of determination in cross-validation (R^2 CV) explains about 15% less of y-variance, meaning that the model is not suitable for quantitative prediction. Nonetheless, the trend is encouraging considering the property we are aiming to predict, and the fact that $T_{1/2}$ values were collected from different authors and measured in possibly varying setups, which could have introduced a degree of error in the measured y. BF_4^- and ClO_4^- are the only two anions represented in this model and, even if being similar in terms of structure and dimensions, a slight shift is found among complexes with the same substituent. This again reflects the importance of the anion in determining the crystal packing and the magnetic properties.

PLS weights plot, reported in Fig. S9 in the ESI,† gives a glimpse on how the variables combine to form a quantitative relationship. Its interpretation is the same as the loadings plot in a PCA model. All the variables are spread almost equally into the plot, without any major observable trend. The farthest, and so the most relevant, variables are T4, T5 (directly correlated), A8 and A9, meaning that bond angles and tortional angles, and not bond distances, play the major role in $T_{1/2}$ prediction. Indeed, once the crystal packing allows the rearrangement of bpp-R ligands toward a more regular octahedron, the Fe–N bond lengths can easily shrink to accommodate the iron (II) in the LS state.

In addition, $T_{1/2}$ seems to show a correlation with the electronic properties of the substituent R. Complexes with Me and S*i*Pr are positioned on the one side, derivatives with H in the middle, and then substituents like Br, I and COOH on the other side of the PLS model. A comparable trend between the σ-Hammett parameter[97] of R and $T_{1/2}$ measured in solution (thus cancelling crystal packing effects) with the variable-temperature Evans method in deuterated solvents[98] was previously observed by analysing 14 $[Fe(bpp\text{-}R)_2](BF_4)_2$ complexes belonging to the congeneric series with R = NO_2, COOH, H, SH, Br, I, Cl, F, Me, SMe, OH, OMe, NH_2 and NMe_2.[63] Finding a similar trend in our study, where a much higher variability is present due to the R groups involved (departure from congeneric series) and the use of structural variables in the solid state where crystal packing interactions are active, is noteworthy. In this PLS regression, the substituents are ordered according to the electronic properties: electron withdrawing groups give the highest $T_{1/2}$ values, while electron donor groups give the lowest $T_{1/2}$ values, with halogens and mild donating groups like Me with intermediate properties being in the middle. Unfortunately, structural data for complexes with NO_2 and NH_2 groups, which represent the two extremes in the solution studies,[63] are not yet available.

The projection of the $T_{1/2}$ values in the PC1 *vs.* PC2 scores plots of the two PCA models constructed with either the 83 HS complexes or the 39 SF HS derivatives also show a clear trend in the distribution across the entire chemical space probed with the PCA models (Fig. S10 in the ESI†). The complexes showing the highest $T_{1/2}$ values (**C06BA** and **X04AA**, *i.e.* bearing COOH and I as substituents) are in the extreme bottom right corner of the plots, as shown in the PLS regression. $T_{1/2}$ then decreases moving in a diagonal fashion toward the centre of the plots until reaching the area of the HS-blocked complexes. This is particularly clear in the case of the SF model, where the challenge given by the solvent lattice is overcome.

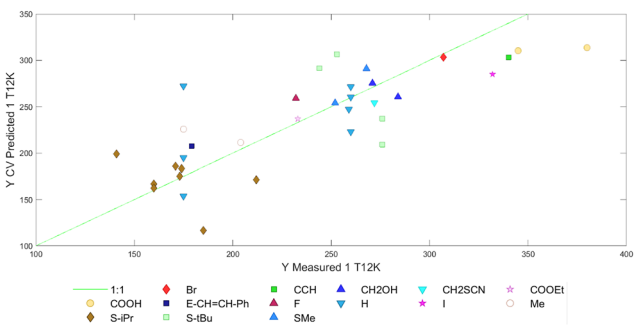

Fig. 5 PLS regression model based on 34 structures of iron(II) complexes: $T_{1/2}$ values measured *vs.* predicted in cross-validation, complexes are classified based on the substituent R.

Conclusions

This work reports the rationalization of the vast body of structural data available for $[Fe(bpp\text{-}R)_2](X)_2$·solvent complexes, by using a novel approach based on multivariate data analysis. The construction of the appropriate dataset for PCA and PLS models involved a great deal of data collection, starting from the literature available and downloading the structural files from the CCDC. Subsequently, the orientation of the molecules to make them comparable in their structural parameters D, A and T proved to be a delicate but fundamental step to avoid errors and the introduction of a source of fictitious variability in the models. Furthermore, the "unexpected" cases, as **C01AA**, enrich the modelling process that is based on capturing the maximum variance among all the complexes.

The PCA models can strikingly distinguish SCO-active complexes from the HS-blocked ones, directly in the solid state. Structural parameters of the iron(II) complexes were also involved in a multivariate regression through the PLS approach. The regression model built towards the prediction of $T_{1/2}$ shows a correlation with the electronic (withdrawing of donor) power of the substituents, in analogy with the previous study in solution,[63] and with the addition of crystal packing effects in the solid state. For sure, more examples of complexes bearing anions X^- other than ClO_4^- and BF_4^- (now accounting for about 80% of the 83 HS compounds available) would enrich the models and make them more comprehensive of the crystal packing effects induced by the cation–anion intermolecular interactions, and this would probably lead to even amplifying the distinction of SCO and HS-blocked complexes in the PCA models.

An important aspect of the approach applied here is that chemometric models can handle, describe, and benefit from the covariance structure among different structural parameters. Thus, considering the structural parameters of the same complex more than once, for example because it is known at various T_{RX}s, is not detrimental for the models. Moreover, PLS regression can cope with highly collinear parameters derived from the various variables, meaning that it is not affected by redundancy, with respect to either samples or descriptors. The possibilities to simultaneously analyse and rationalize all available structural data in a single model and, at the same time, to gather different degrees of details refining specific models on restricted congeneric series, *e.g.* anions, substituents, *etc*., offer the desired flexibility to deepen the knowledge of the interplay of all the main structural motifs and related intermolecular interactions.

It is possible to implement the models by introducing other families of iron(II) complexes with two *mer*-coordinated neutral tridentate ligands to gather information on the donor sets and this will be the object of future research. The derived models can also be directly used to estimate other isostructural complexes for which the same structural parameters (A, T, D) can be defined, *e.g.* holding a different metal centre. In addition, the approach is very general and can be adopted with any complex set whose structural information is available in the CCDC. This opens the road to an innovative branch of data analysis from the synergistic match of crystallography, with over one million available crystal structures, and chemometrics, with the potency of dealing with big data.

Conflicts of interest

There are no conflicts to declare.

Acknowledgements

This research has been funded by the Royal Society of Chemistry through the RSC Research Fund grant no. R19-0504 entitled '*Nitrogen-donor ligands for new molecular iron(II) spin crossover complexes and cobalt(II) single-molecule magnets*', and by the Dipartimento di Scienze Chimiche e Geologiche of the Università degli Studi di Modena e Reggio Emilia through the Fondo Dipartimentale per la Ricerca 2020 (FDR2020).

References

1 L. Bogani and W. Wernsdorfer, Molecular spintronics using single-molecule magnets, *Nat. Mater.*, 2008, **7**, 179–186.
2 M. N. Leuenberger and D. Loss, Quantum computing in molecular magnets, *Nature*, 2001, **410**, 789–793.
3 J. Lehmann, A. Gaita-Ariño, E. Coronado and D. Loss, Quantum computing with molecular spin systems, *J. Mater. Chem.*, 2009, **19**, 1672–1677.
4 O. Kahn, Spin-Transition Polymers: From Molecular Materials Toward Memory Devices, *Science*, 1998, **279**, 44–48.
5 H. Douib, L. Cornet, J. F. Gonzalez, E. Trzop, V. Dorcet, A. Gouasmia, L. Ouahab, O. Cador and F. Pointillart, Spin-Crossover and Field-Induced Single-Molecule Magnet Behaviour in Metal(II)-Dipyrazolylpyridine Complexes: Spin-Crossover and Field-Induced Single-Molecule Magnet Behaviour in Metal(II)-Dipyrazolylpyridine Complexes, *Eur. J. Inorg. Chem.*, 2018, 4452–4457.
6 M. Nihei, T. Shiga, Y. Maeda and H. Oshio, Spin crossover iron(III) complexes, *Coord. Chem. Rev.*, 2007, **251**, 2606–2621.
7 *Spin-crossover materials: properties and applications*, ed. M. A. Halcrow, Wiley, Chichester, 2013.
8 M. A. Halcrow, Structure:function relationships in molecular spin-crossover complexes, *Chem. Soc. Rev.*, 2011, **40**, 4119–4142.
9 G. Chastanet, M. Lorenc, R. Bertoni and C. Desplanches, Light-induced spin crossover—Solution and solid-state processes, *C. R. Chim.*, 2018, **21**, 1075–1094.
10 G. Chastanet, C. Desplanches, C. Baldé, P. Rosa, M. Marchivie and P. Guionneau, A critical review of the T(LIESST) temperature in spin crossover materials – What it is and what it is not, *Chem. Sq.*, 2018, **2**, 2.
11 E. Fernandez-Bartolome, A. Martinez-Martinez, E. Resines-Urien, L. Piñeiro-Lopez and J. S. Costa, Reversible single-crystal-to-single-crystal transformations in coordination compounds induced by external stimuli, *Coord. Chem. Rev.*, 2022, **452**, 214281.
12 D. Unruh, P. Homenya, M. Kumar, R. Sindelar, Y. Garcia and F. Renz, Spin state switching of metal complexes by visible light or hard X-rays, *Dalton Trans.*, 2016, **45**, 14008–14018.
13 A. Bousseksou, G. Molnár, L. Salmon and W. Nicolazzi, Molecular spin crossover phenomenon: recent achievements and prospects, *Chem. Soc. Rev.*, 2011, **40**, 3313–3335.
14 W. R. Scheidt and C. A. Reed, Spin-state/stereochemical relationships in iron porphyrins: implications for the hemoproteins, *Chem. Rev.*, 1981, **81**, 543–555.

15 K. D. Sutherlin, B. S. Rivard, L. H. Böttger, L. V. Liu, M. S. Rogers, M. Srnec, K. Park, Y. Yoda, S. Kitao, Y. Kobayashi, M. Saito, M. Seto, M. Hu, J. Zhao, J. D. Lipscomb and E. I. Solomon, NRVS Studies of the Peroxide Shunt Intermediate in a Rieske Dioxygenase and Its Relation to the Native $Fe^{II}O_2$ Reaction, *J. Am. Chem. Soc.*, 2018, **140**, 5544–5559.

16 E. I. Solomon, D. E. DeWeese and J. T. Babicz, Mechanisms of O_2 Activation by Mononuclear Non-Heme Iron Enzymes, *Biochemistry*, 2021, **60**, 3497–3506.

17 P. Gütlich, A. Hauser and H. Spiering, Thermal and Optical Switching of Iron(II) Complexes, *Angew. Chem., Int. Ed. Engl.*, 1994, **33**, 2024–2054.

18 P. Gütlich, Y. Garcia and H. A. Goodwin, Spin crossover phenomena in Fe(II) complexes, *Chem. Soc. Rev.*, 2000, **29**, 419–427.

19 O. Kahn, J. Kröber and C. Jay, Spin Transition Molecular Materials for displays and data recording, *Adv. Mater.*, 1992, **4**, 718–728.

20 G. Bovo, I. Bräunlich, W. R. Caseri, N. Stingelin, T. D. Anthopoulos, K. G. Sandeman, D. D. C. Bradley and P. N. Stavrinou, Room temperature dielectric bistability in solution-processed spin crossover polymer thin films, *J. Mater. Chem. C*, 2016, **4**, 6240–6248.

21 M. Matsuda and H. Tajima, Thin Film of a Spin Crossover Complex $[Fe(dpp)_2](BF_4)_2$, *Chem. Lett.*, 2007, **36**, 700–701.

22 S. Xue, Y. Guo, A. Rotaru, H. Müller-Bunz, G. G. Morgan, E. Trzop, E. Collet, J. Oláh and Y. Garcia, Spin Crossover Behavior in a Homologous Series of Iron(II) Complexes Based on Functionalized Bipyridyl Ligands, *Inorg. Chem.*, 2018, **57**, 9880–9891.

23 Y.-H. Luo, M. Nihei, G.-J. Wen, B.-W. Sun and H. Oshio, Ambient-Temperature Spin-State Switching Achieved by Protonation of the Amino Group in $[Fe(H_2Bpz_2)_2(bipy\text{-}NH_2)]$, *Inorg. Chem.*, 2016, **55**, 8147–8152.

24 J. P. Janet, L. Chan and H. J. Kulik, Accelerating Chemical Discovery with Machine Learning: Simulated Evolution of Spin Crossover Complexes with an Artificial Neural Network, *J. Phys. Chem. Lett.*, 2018, **9**, 1064–1071.

25 M. G. Taylor, T. Yang, S. Lin, A. Nandy, J. P. Janet, C. Duan and H. J. Kulik, Seeing Is Believing: Experimental Spin States from Machine Learning Model Structure Predictions, *J. Phys. Chem. A*, 2020, **124**, 3286–3299.

26 J. M. Holland, C. A. Kilner, M. Thornton-Pett, M. A. Halcrow, J. A. McAllister and Z. Lu, An unusual abrupt thermal spin-state transition in $[FeL_2][BF_4]_2$ [L = 2,6-di(pyrazol-1-yl)pyridine], *Chem. Commun.*, 2001, 577–578.

27 J. M. Holland, J. A. McAllister, C. A. Kilner, M. Thornton-Pett, A. J. Bridgeman and M. A. Halcrow, Stereochemical effects on the spin-state transition shown by salts of $[FeL_2]^{2+}$ [L = 2,6-di(pyrazol-1-yl)pyridine], *J. Chem. Soc., Dalton Trans.*, 2002, 548–554.

28 V. A. Money, I. Radosavljevic Evans, M. A. Halcrow, A. E. Goeta and J. A. K. Howard, Light induced excited high spin-state trapping in $[FeL_2](BF_4)_2$ (L = 2,6-di(pyrazol-1-yl) pyridine), *Chem. Commun.*, 2003, 158–159.

29 V. A. Money, J. Elhaïk, M. A. Halcrow and J. A. K. Howard, The thermal and light induced spin transition in $[FeL_2](BF_4)_2$ (L = 2,6-dipyrazol-1-yl-4-hydroxymethylpyridine), *Dalton Trans.*, 2004, 1516–1518.

30 J. Elhaïk, D. J. Evans, C. A. Kilner and M. A. Halcrow, A structural, magnetic and Mössbauer spectroscopic study of an unusual angular Jahn–Teller distortion in a series of high-spin iron(II) complexes, *Dalton Trans.*, 2005, 1693–1700.

31 J. Elhaïk, C. A. Kilner and M. A. Halcrow, Structural diversity in iron(II) complexes of 2,6-di(pyrazol-1-yl)pyridine and 2,6-di(3-methylpyrazol-1-yl)pyridine, *Dalton Trans.*, 2006, 823–830.

32 C. Carbonera, J. Sánchez Costa, V. A. Money, J. Elhaïk, J. A. K. Howard, M. A. Halcrow and J.-F. Létard, Photomagnetic properties of iron(II) spin crossover complexes of 2,6-dipyrazolylpyridine and 2,6-dipyrazolylpyrazine ligands, *Dalton Trans.*, 2006, 3058–3066.

33 C. Rajadurai, F. Schramm, S. Brink, O. Fuhr, M. Ghafari, R. Kruk and M. Ruben, Spin Transition in a Chainlike Supramolecular Iron(II) Complex, *Inorg. Chem.*, 2006, **45**, 10019–10021.

34 C. Carbonera, C. A. Kilner, J.-F. Létard and M. A. Halcrow, Anion doping as a probe of cooperativity in the molecular spin-crossover compound $[FeL_2][BF_4]_2$ (L = 2,6-di{pyrazol-1-yl}pyridine), *Dalton Trans.*, 2007, 1284–1292.

35 C. Rajadurai, Z. Qu, O. Fuhr, B. Gopalan, R. Kruk, M. Ghafari and M. Ruben, Lattice-solvent controlled spin transitions in iron(II) complexes, *Dalton Trans.*, 2007, 3531.

36 M. Nihei, L. Han and H. Oshio, Magnetic Bistability and Single-Crystal-to-Single-Crystal Transformation Induced by Guest Desorption, *J. Am. Chem. Soc.*, 2007, **129**, 5312–5313.

37 M. Nihei, T. Maeshima, Y. Kose and H. Oshio, Synthesis, structure and magnetic properties of an iron(II) complex with nitronyl nitroxides, *Polyhedron*, 2007, **26**, 1993–1996.

38 N. T. Madhu, I. Salitros, F. Schramm, S. Klyatskaya, O. Fuhr and M. Ruben, Above room temperature spin transition in a series of iron(II) bis(pyrazolyl)pyridine compounds, *C. R. Chim.*, 2008, **11**, 1166–1174.

39 R. Chandrasekar, F. Schramm, O. Fuhr and M. Ruben, An Iron(II) Spin-Transition Compound with Thiol Anchoring Groups, *Eur. J. Inorg. Chem.*, 2008, 2649–2653.

40 M. Nihei, L. Han, H. Tahira and H. Oshio, Syntheses, structures and magnetic properties of iron(II) complexes with bulky tridentate ligands, *Inorg. Chim. Acta*, 2008, **361**, 3926–3930.

41 M. A. Halcrow, Iron(II) complexes of 2,6-di(pyrazol-1-yl)pyridines—A versatile system for spin-crossover research, *Coord. Chem. Rev.*, 2009, **253**, 2493–2514.

42 C. A. Tovee, C. A. Kilner, J. A. Thomas and M. A. Halcrow, Co-crystallising two functional complex molecules in a terpyridine embrace lattice, *CrystEngComm*, 2009, **11**, 2069–2077.

43 M. Haryono, F. W. Heinemann, K. Petukhov, K. Gieb, P. Müller and A. Grohmann, Parallel Crystallization of a "Static" and a Spin-Crossover Polymorph of an Iron(II)

Complex from the Same Solution, *Eur. J. Inorg. Chem.*, 2009, 2136–2143.

44 I. Šalitroš, J. Pavlik, R. Boča, O. Fuhr, C. Rajadurai and M. Ruben, Supramolecular lattice-solvent control of iron(II) spin transition parameters, *CrystEngComm*, 2010, **12**, 2361–2368.

45 M. Nihei, H. Tahira, N. Takahashi, Y. Otake, Y. Yamamura, K. Saito and H. Oshio, Multiple Bistability and Tristability with Dual Spin-State Conversions in $[Fe(dpp)_2][Ni(mnt)_2]_2 \cdot MeNO_2$, *J. Am. Chem. Soc.*, 2010, **132**, 3553–3560.

46 Y. Hasegawa, K. Takahashi, S. Kume and H. Nishihara, Complete solid state photoisomerization of bis(dipyrazolylstyrylpyridine)iron(II) to change magnetic properties, *Chem. Commun.*, 2011, **47**, 6846–6848.

47 M. Nihei, N. Takahashi, H. Nishikawa and H. Oshio, Spin-crossover behavior and electrical conduction property in iron(II) complexes with tetrathiafulvalene moieties, *Dalton Trans.*, 2011, **40**, 2154–2156.

48 R. González-Prieto, B. Fleury, F. Schramm, G. Zoppellaro, R. Chandrasekar, O. Fuhr, S. Lebedkin, M. Kappes and M. Ruben, Tuning the spin-transition properties of pyrene-decorated 2,6-bispyrazolylpyridine based Fe(II) complexes, *Dalton Trans.*, 2011, **40**, 7564–7570.

49 I. Šalitroš, O. Fuhr, A. Eichhöfer, R. Kruk, J. Pavlik, L. Dlháň, R. Boča and M. Ruben, The interplay of iron(II) spin transition and polymorphism, *Dalton Trans.*, 2012, **41**, 5163–5171.

50 K. Takahashi, Y. Hasegawa, R. Sakamoto, M. Nishikawa, S. Kume, E. Nishibori and H. Nishihara, Solid-State Ligand-Driven Light-Induced Spin Change at Ambient Temperatures in Bis(dipyrazolylstyrylpyridine)iron(II) Complexes, *Inorg. Chem.*, 2012, **51**, 5188–5198.

51 I. Šalitroš, O. Fuhr, R. Kruk, J. Pavlik, L. Pogány, B. Schäfer, M. Tatarko, R. Boča, W. Linert and M. Ruben, Thermal and Photoinduced Spin Crossover in a Mononuclear Iron(II) Complex with a Bis(pyrazolyl)pyridine Type of Ligand, *Eur. J. Inorg. Chem.*, 2013, 1049–1057.

52 Y. Hasegawa, R. Sakamoto, K. Takahashi and H. Nishihara, Bis[(*E*)-2,6-bis(1*H*-pyrazol-1-yl)-4-styrylpyridine]iron(II) Complex: Relationship between Thermal Spin Crossover and Crystal Solvent, *Inorg. Chem.*, 2013, **52**, 1658–1665.

53 R. J. Davidson, E. W. Ainscough, A. M. Brodie, M. R. Waterland, H. R. Allcock, M. D. Hindenlang, B. Moubaraki, K. S. Murray, K. C. Gordon, R. Horvath and G. N. L. Jameson, A behavioural difference between an iron(II) grafted polyphosphazene and its small molecule cyclophosphazene analogue, *Inorg. Chem. Commun.*, 2013, **37**, 158–161.

54 A. Abhervé, M. Clemente-León, E. Coronado, C. J. Gómez-García and M. López-Jordà, A spin-crossover complex based on a 2,6-bis(pyrazol-1-yl)pyridine (1-bpp) ligand functionalized with a carboxylate group, *Dalton Trans.*, 2014, **43**, 9406–9409.

55 L. J. Kershaw Cook, H. J. Shepherd, T. P. Comyn, C. Baldé, O. Cespedes, G. Chastanet and M. A. Halcrow, Decoupled Spin Crossover and Structural Phase Transition in a Molecular Iron(II) Complex, *Chem. – Eur. J.*, 2015, **21**, 4805–4816.

56 L. J. Kershaw Cook, R. Mohammed, G. Sherborne, T. D. Roberts, S. Alvarez and M. A. Halcrow, Spin state behavior of iron(II)/dipyrazolylpyridine complexes. New insights from crystallographic and solution measurements, *Coord. Chem. Rev.*, 2015, **289–290**, 2–12.

57 L. J. Kershaw Cook, J. Fisher, L. P. Harding and M. A. Halcrow, An iron(II) spin-crossover metallacycle from a back-to-back bis-[dipyrazolylpyridine], *Dalton Trans.*, 2015, **44**, 9417–9425.

58 L. J. Kershaw Cook, R. Kulmaczewski, S. A. Barrett and M. A. Halcrow, Iron(II) complexes of 4-sulfanyl-, 4-sulfinyl- and 4-sulfonyl-2,6-dipyrazolylpyridine ligands. A subtle interplay between spin-crossover and crystallographic phase changes, *Inorg. Chem. Front.*, 2015, **2**, 662–670.

59 L. J. Kershaw Cook, F. L. Thorp-Greenwood, T. P. Comyn, O. Cespedes, G. Chastanet and M. A. Halcrow, Unexpected Spin-Crossover and a Low-Pressure Phase Change in an Iron(II)/Dipyrazolylpyridine Complex Exhibiting a High-Spin Jahn–Teller Distortion, *Inorg. Chem.*, 2015, **54**, 6319–6330.

60 L. Pukenas, F. Benn, E. Lovell, A. Santoro, L. J. Kershaw Cook, M. A. Halcrow and S. D. Evans, Bead-like structures and self-assembled monolayers from 2,6-dipyrazolylpyridines and their iron(II) complexes, *J. Mater. Chem. C*, 2015, **3**, 7890–7896.

61 A. Abhervé, M. Palacios-Corella, J. M. Clemente-Juan, R. Marx, P. Neugebauer, J. van Slageren, M. Clemente-León and E. Coronado, Bimetallic Mn^{III}–Fe^{II} hybrid complexes formed by a functionalized Mn^{III} Anderson polyoxometalate coordinated to Fe^{II}: observation of a field-induced slow relaxation of magnetization in the Mn^{III} centres and a photoinduced spin-crossover in the Fe^{II} centres, *J. Mater. Chem. C*, 2015, **3**, 7936–7945.

62 L. J. Kershaw Cook and M. A. Halcrow, Synthesis of 4-Hydroxy-2,6-di(pyrazol-1-yl)pyridine, and the Spin State Behaviour of Its Iron(II) Complex Salts, *Magnetochemistry*, 2015, **1**, 3–16.

63 L. J. Kershaw Cook, R. Kulmaczewski, R. Mohammed, S. Dudley, S. A. Barrett, M. A. Little, R. J. Deeth and M. A. Halcrow, A Unified Treatment of the Relationship Between Ligand Substituents and Spin State in a Family of Iron(II) Complexes, *Angew. Chem., Int. Ed.*, 2016, **55**, 4327–4331.

64 L. J. Kershaw Cook, R. Kulmaczewski, O. Cespedes and M. A. Halcrow, Different Spin-State Behaviors in Isostructural Solvates of a Molecular Iron(II) Complex, *Chem. – Eur. J.*, 2016, **22**, 1789–1799.

65 A. Abhervé, M. J. Recio-Carretero, M. López-Jordà, J. M. Clemente-Juan, J. Canet-Ferrer, A. Cantarero, M. Clemente-León and E. Coronado, Nonanuclear Spin-Crossover Complex Containing Iron(II) and Iron(III) Based on a 2,6-Bis(pyrazol-1-yl)pyridine Ligand Functionalized with a Carboxylate Group, *Inorg. Chem.*, 2016, **55**, 9361–9367.

66 R. Kulmaczewski, E. Trzop, L. J. Kershaw Cook, E. Collet, G. Chastanet and M. A. Halcrow, The role of symmetry breaking in the structural trapping of light-induced excited spin states, *Chem. Commun.*, 2017, **53**, 13268–13271.

67 B. Schäfer, T. Bauer, I. Faus, J. A. Wolny, F. Dahms, O. Fuhr, S. Lebedkin, H.-C. Wille, K. Schlage, K. Chevalier, F. Rupp, R. Diller, V. Schünemann, M. M. Kappes and M. Ruben, A luminescent Pt_2Fe spin crossover complex, *Dalton Trans.*, 2017, **46**, 2289–2302.

68 N. Bridonneau, L. Rigamonti, G. Poneti, D. Pinkowicz, A. Forni and A. Cornia, Evidence of crystal packing effects in stabilizing high or low spin states of iron(II) complexes with functionalized 2,6-bis(pyrazol-1-yl)pyridine ligands, *Dalton Trans.*, 2017, **46**, 4075–4085.

69 K. S. Kumar, I. Šalitroš, E. Moreno-Pineda and M. Ruben, Spacer type mediated tunable spin crossover (SCO) characteristics of pyrene decorated 2,6-bis(pyrazol-1-yl)pyridine (bpp) based Fe(ii) molecular spintronic modules, *Dalton Trans.*, 2017, **46**, 9765–9768.

70 I. Capel Berdiell, R. Kulmaczewski, O. Cespedes and M. A. Halcrow, An Incomplete Spin Transition Associated with a Z′ = 1 → Z′ = 24 Crystallographic Symmetry Breaking, *Chem. – Eur. J.*, 2018, **24**, 5055–5059.

71 V. García-López, M. Palacios-Corella, A. Abhervé, I. Pellicer-Carreño, C. Desplanches, M. Clemente-León and E. Coronado, Spin-crossover compounds based on iron(II) complexes of 2,6-bis(pyrazol-1-yl)pyridine (bpp) functionalized with carboxylic acid and ethyl carboxylic acid, *Dalton Trans.*, 2018, **47**, 16958–16968.

72 K. S. Kumar, I. Šalitroš, N. Suryadevara, E. Moreno-Pineda and M. Ruben, Supramolecular Interaction Tuning of Spin-Crossover in Pyrene/Fullerene (C_{60}) Tethered Fe^{II}-2,6-Di(pyrazol-1-yl)pyridine Complexes: Towards Switchable Molecular Devices, *Eur. J. Inorg. Chem.*, 2018, 5091–5097.

73 I. Galadzhun, R. Kulmaczewski, O. Cespedes, M. Yamada, N. Yoshinari, T. Konno and M. A. Halcrow, 2,6-Bis(pyrazol-1-yl)pyridine-4-carboxylate Esters with Alkyl Chain Substituents and Their Iron(II) Complexes, *Inorg. Chem.*, 2018, **57**, 13761–13771.

74 M. Attwood, H. Akutsu, L. Martin, D. Cruickshank and S. S. Turner, Above room temperature spin crossover in thioamide-functionalised 2,6-bis(pyrazol-1-yl)pyridine iron(II) complexes, *Dalton Trans.*, 2019, **48**, 90–98.

75 K. S. Kumar, B. Heinrich, S. Vela, E. Moreno-Pineda, C. Bailly and M. Ruben, Bi-stable spin-crossover characteristics of a highly distorted $[Fe(1\text{-BPP-COOC}_2H_5)_2](ClO_4)_2\cdot CH_3CN$ complex, *Dalton Trans.*, 2019, **48**, 3825–3830.

76 I. Šalitroš, R. Herchel, O. Fuhr, R. González-Prieto and M. Ruben, Polynuclear Iron(II) Complexes with 2,6-Bis(pyrazol-1-yl)pyridine-anthracene Ligands Exhibiting Highly Distorted High-Spin Centers, *Inorg. Chem.*, 2019, **58**, 4310–4319.

77 I. Galadzhun, R. Kulmaczewski and M. A. Halcrow, Five 2,6-Di(pyrazol-1-yl)pyridine-4-carboxylate Esters, and the Spin States of their Iron(II) Complexes, *Magnetochemistry*, 2019, **5**, 9.

78 V. García-López, M. Palacios-Corella, M. Clemente-León and E. Coronado, Fe(II) spin crossover complexes of a derivative of 2,6-bis(pyrazol-1-yl)pyridine (1-bpp) functionalized with a carboxylic acid in the 3-pyridyl position, *Polyhedron*, 2019, **170**, 95–100.

79 K. Senthil Kumar, N. Del Giudice, B. Heinrich, L. Douce and M. Ruben, Bistable spin-crossover in a new series of $[Fe(BPP\text{-}R)_2]^{2+}$ (BPP = 2,6-bis(pyrazol-1-yl)pyridine; R = CN) complexes, *Dalton Trans.*, 2020, **49**, 14258–14267.

80 I. Capel Berdiell, R. Kulmaczewski, S. L. Warriner, O. Cespedes and M. A. Halcrow, Iron and Silver Complexes of 4–(Imidazol–1–yl)–2,6–di(pyrazol–1–yl)–pyridine (*L*), Including a $[Fe_3(\mu\text{–}F)_2F_6L_8]^+$ Assembly, *Eur. J. Inorg. Chem.*, 2020, 4334–4340.

81 R. Kulmaczewski, E. Trzop, E. Collet, S. Vela and M. A. Halcrow, Structure:function relationships for thermal and light-induced spin-crossover in isomorphous molecular materials, *J. Mater. Chem. C*, 2020, **8**, 8420–8429.

82 R. Kulmaczewski, F. Bamiduro, N. Shahid, O. Cespedes and M. A. Halcrow, Structural Transformations and Spin–Crossover in $[FeL_2]^{2+}$ Salts (*L* = 4–{*tert*–Butylsulfanyl}–2,6–di{pyrazol–1–yl}pyridine): The Influence of Bulky Ligand Substituents, *Chem. – Eur. J.*, 2021, **27**, 2082–2092.

83 I. Capel Berdiell, V. García-López, M. J. Howard, M. Clemente-León and M. A. Halcrow, The effect of tether groups on the spin states of iron(II)/bis[2,6-di(pyrazol-1-yl)pyridine] complexes, *Dalton Trans.*, 2021, **50**, 7417–7426.

84 M. A. Halcrow, I. Capel Berdiell, C. M. Pask and R. Kulmaczewski, Relationship between the Molecular Structure and Switching Temperature in a Library of Spin-Crossover Molecular Materials, *Inorg. Chem.*, 2019, **58**, 9811–9821.

85 D. J. Durand and N. Fey, Computational Ligand Descriptors for Catalyst Design, *Chem. Rev.*, 2019, **119**, 6561–6594.

86 D. J. Durand and N. Fey, Building a Toolbox for the Analysis and Prediction of Ligand and Catalyst Effects in Organometallic Catalysis, *Acc. Chem. Res.*, 2021, **54**, 837–848.

87 I. T. Jolliffe, *Principal component analysis*, Springer, New York, 2nd edn, 2002.

88 P. Geladi and B. R. Kowalski, Partial least-squares regression: a tutorial, *Anal. Chim. Acta*, 1986, **185**, 1–17.

89 L. Rigamonti, N. Bridonneau, G. Poneti, L. Tesi, L. Sorace, D. Pinkowicz, J. Jover, E. Ruiz, R. Sessoli and A. Cornia, A Pseudo-Octahedral Cobalt(II) Complex with bis-Pyrazolylpyridine Ligands Acting as a Zero-Field Single-Molecule Magnet with Easy Axis Anisotropy, *Chem. – Eur. J.*, 2018, **24**, 8857–8868.

90 F. H. Allen and R. Taylor, Research applications of the Cambridge Structural Database (CSD), *Chem. Soc. Rev.*, 2004, **33**, 463–475.

91 S. E. Harris, A. G. Orpen, I. J. Bruno and R. Taylor, Factors Affecting *d*-Block Metal–Ligand Bond Lengths: Toward an Automated Library of Molecular Geometry for Metal Complexes, *J. Chem. Inf. Model.*, 2005, **45**, 1727–1748.

92 N. Fey, S. E. Harris, J. N. Harvey and A. G. Orpen, Adding Value to Crystallographically-Derived Knowledge Bases, *J. Chem. Inf. Model.*, 2006, **46**, 912–929.

93 D. A. V. Morton and A. G. Orpen, Structural systematics. Part 4. Conformations of the diphosphine ligands in $M_2(\mu\text{-}Ph_2PCH_2PPh_2)$ and $M(Ph_2PCH_2CH_2PPh_2)$ complexes, *J. Chem. Soc., Dalton Trans.*, 1992, 641–653.

94 Y. Marcus, The Molar Volumes of Ions in Solution, Part 7. Electrostriction and Hydration Numbers of Aqueous Polyatomic Anions at 25 °C, *J. Phys. Chem. B*, 2014, **118**, 2172–2175.

95 M. Hostettler, K. W. Törnroos, D. Chernyshov, B. Vangdal and H.-B. Bürgi, Challenges in Engineering Spin Crossover: Structures and Magnetic Properties of Six Alcohol Solvates of Iron(II) Tris(2-picolylamine) Dichloride, *Angew. Chem., Int. Ed.*, 2004, **43**, 4589–4594.

96 R. Kulmaczewski, M. J. Howard and M. A. Halcrow, Influence of ligand substituent conformation on the spin state of an iron(II)/di(pyrazol-1-yl)pyridine complex, *Dalton Trans.*, 2021, **50**, 3464–3467.

97 P. Teesdale-Spittle, Advanced organic chemistry: Reactions, mechanisms and structure, 4th edn, in *Appl. Organomet. Chem*, 1992, vol. 7, pp. 293–293.

98 E. M. Schubert, Utilizing the Evans method with a superconducting NMR spectrometer in the undergraduate laboratory, *J. Chem. Educ.*, 1992, **69**, 62.